Supporting Information

Synergistic enhancement of photovoltaic performance for TiO2 photoanode by incorporating with Dawson-type polyoxometalate and gold nanoparticles

Lihao Wang, [a] *Lin Xu,* [a,*] *Zhongcheng Mu, Chungang Wang, Zhixia Sun*

Materials

Preparation of $K_6P_2W_{18}O_{62}$: $Na_2WO_4 \cdot 2H_2O$ (100g) was added to 350ml of water, and the solution was heated to boiling. Then 150ml of 85% H_3PO_4 was solwly added to the boiling solution, and the resulting yellow-green solution was refluxed for 5-13h. The solution was cooled, and the product was precipitated by addition of 100g of solid KCl. The light green precipitate was collected, redissolved in a minimum amount of hot water, and allowed to crystallize at 5℃ overnight. Cyclic voltammertry and UV-vis adsorption spectra were used to identify the product, which were shown in Fig. S1 and Fig. S2.

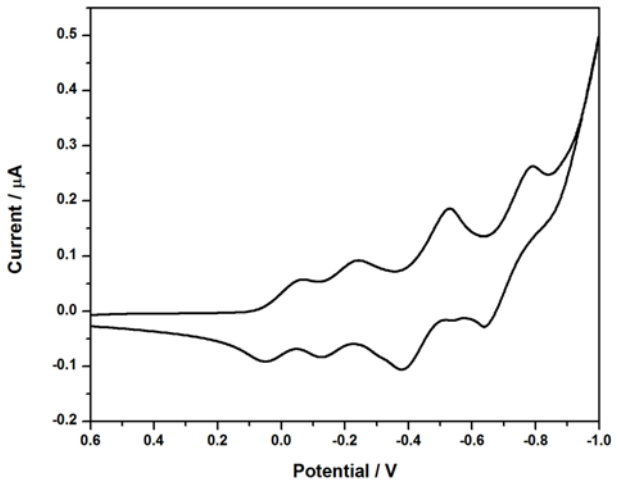

Fig. S1 Cyclic voltammograms of P_2W_{18}.

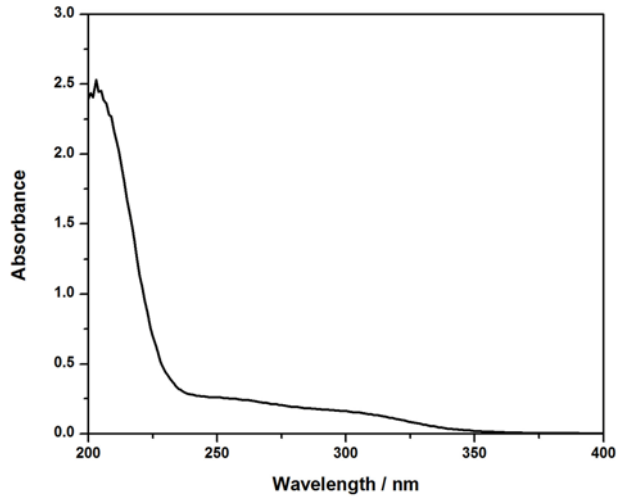

Fig. S2 UV-vis aborption spectra of P_2W_{18}.

Preparation of TiO_2: TiO_2 colloid solutions were prepared by hydrolysis of titanium isopropoxide, $Ti(OCH(CH_3)_2)_4$, as follows: 25ml $Ti(OCH(CH_3)_2)_4$ was added to dropping funnel containing 0.4ml of 2-propanol. The mixture was added slowly to 15ml deionized water, stirring vigorously. During the hydrolysis, 0.1ml of 70% HNO_3 was added. The mixture was then stirred for 8h at ~80℃. As shown in Fig. S3 and Fig. S4, they were edscribed by X-ray diffraction (XRD) analysis and Transmission electron microscopy (TEM) image.

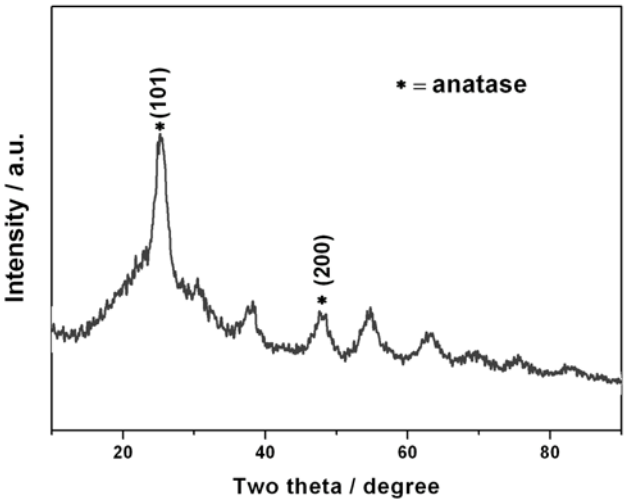

Fig. S3. XRD pattern of TiO_2 colloids.

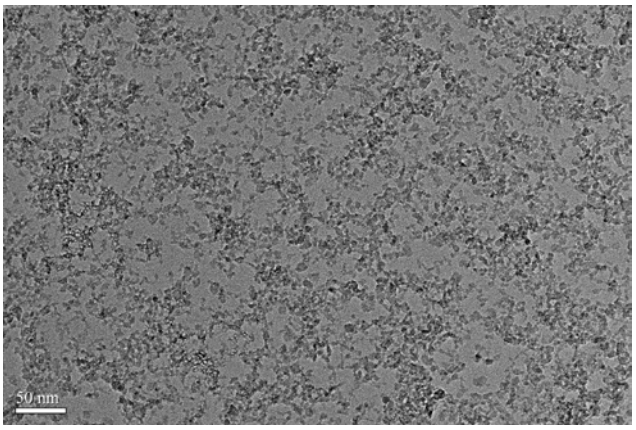

Fig. S4. TEM image of TiO_2 colloids.

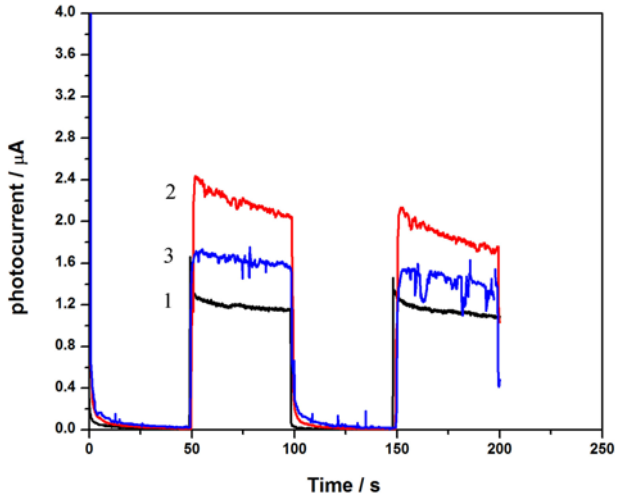

Fig. S5 Photocurrent versus time curves of the $(P_2W_{18}/TiO_2)_n$ films of different layers (n=1-3).

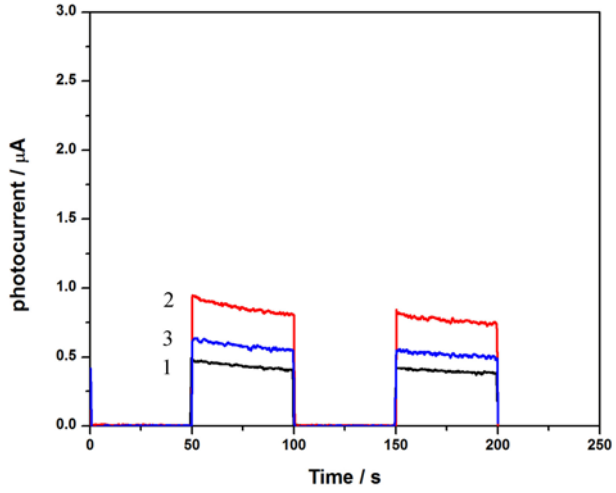

Fig. S6 Photocurrent versus time curves of the $(PSS/TiO_2)_n$ films of different layers (n=1-3).

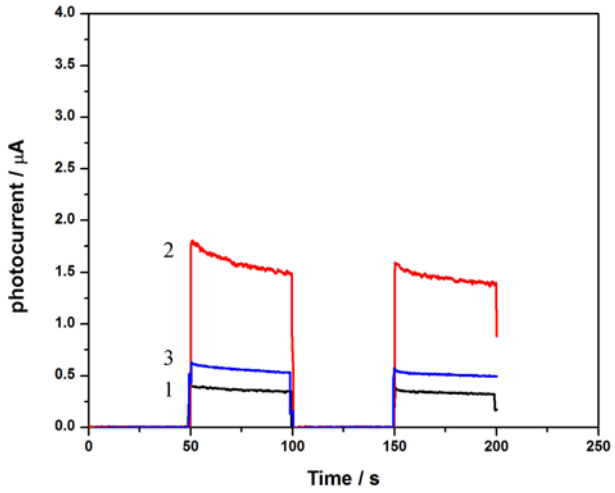

Fig. S7 Photocurrent versus time curves of the $(PSS/TiO_2/PSS/Au)_n$ films of different layers (n=1-3).

Photoelectrochemical Oxidation of Methanol

To explore the photoelectrocatalytic activity of the LbL films, the photoelectrooxidation process of methanol was investigated at a constant bias of 0.5 V under Xe lamp irradiation. Fig. S8A shows the photocurrents obtained for the $(PSS/TiO2)_2$ film (a), the $(P_2W_{18}/TiO_2)2$ film (b), and the $(P_2W_{18}/TiO_2/P_2W_{18}/Au)_2$ film (c) in different concentrations of methanol. The presence of methanol increases the photocurrent responses of these films, and, in particular, the $(P_2W_{18}/TiO_2/P_2W_{18}/Au)_2$ film has the highest photocurrent in each concentration of methanol. This indicates that the $(P_2W_{18}/TiO_2/P2W_{18}/Au)_2$ film possesses a more significant photoelectrooxidation activity for methanol. It is well known that the photogenerated hole can oxidate methanol either by formation of reactive hydroxyl radicals or by direct charge transfer. From comparison of the concentration dependence on the photocurrent (Fig. S8A) with model predictions (ref. *J. Phys. Chem. B*, 1999, **103**, 5505-5511.), we propose that the increase in the photocurrent measured in the presence of methanol can be attributed to direct hole transfer, which is similar to the results reported by Marugán and coworkers (ref. *Appl. Catal. B*, 2009, **89**, 273-283.). Furthermore, Fig. S8B displays the concentration /photocurrent (C/I_{ph}) versus concentration plot for methanol oxidation at the $(PSS/TiO_2)_2$ film (a), the $(P_2W_{18}/TiO_2)_2$ film (b), and the $(P_2W_{18}/TiO_2/P_2W_{18}/Au)_2$ film. The kinetics plot of the photoelectrooxidation of methanol appears linearly in the 0.1-0.5 M range, which obeys the Langmuir-Hinselwood kinetics equation (ref. *Electrochim. Acta*, 2006, **51**, 2076-2087.).

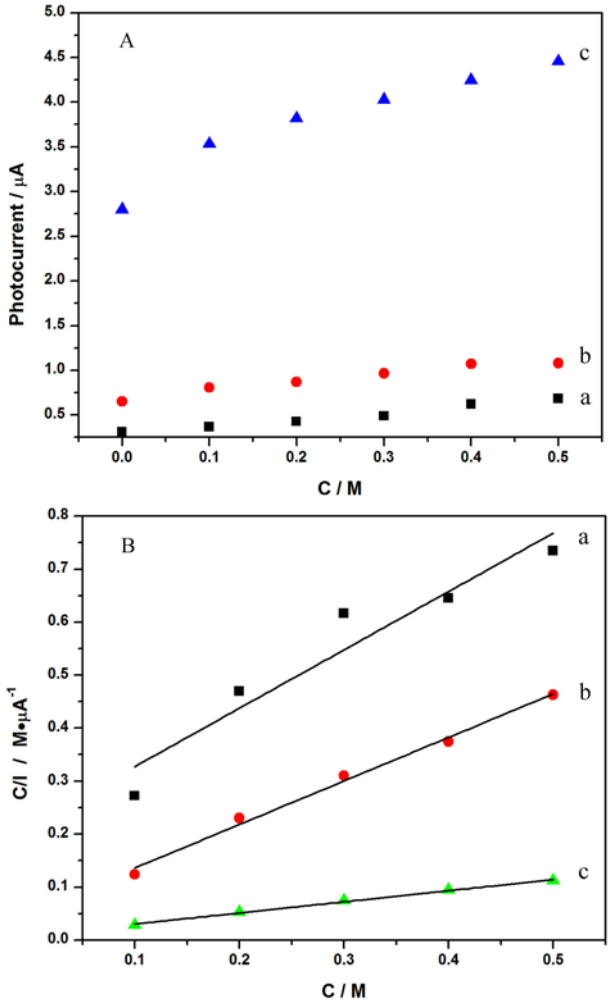

Fig. S8 (A) Dependence of photocurrent on methanol concentration of (a) the $(PSS/TiO_2)_2$ film, (b) the $(P_2W_{18}/TiO_2)_2$ film, and (c) the $(P_2W_{18}/TiO_2/P_2W_{18}/Au)_2$ film in 0.1 Na_2SO_4. (B) Plot of methanol concentration to photocurrent, C/I_{ph}, vs C for (a) the $(PSS/TiO_2)_2$ film, (b) the $(P_2W_{18}/TiO_2)_2$ film, and (c) the $(P_2W_{18}/TiO_2/P_2W_{18}/Au)_2$ film.

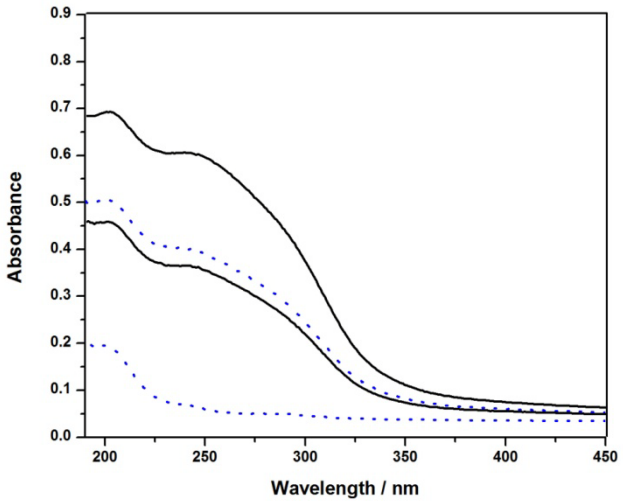

Fig. S9 UV-vis absorption spectra of multilayer films $(P_2W_{18}/TiO_2)_2$ (from lower to upper curves). The dashed line represents spectra after P_2W_{18} deposition, the solid line represents spectra after TiO_2 deposition.

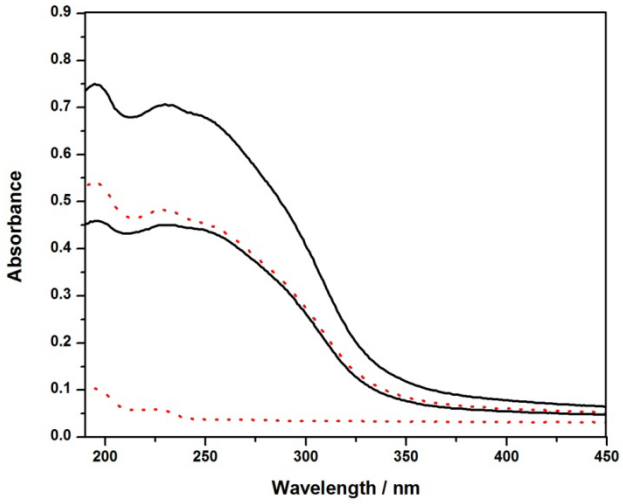

Fig. S10 UV-vis absorption spectra of multilayer films $(PSS/TiO_2)_2$ (from lower to upper curves). The dashed line represents spectra after PSS deposition, the solid line represents spectra after TiO_2 deposition.

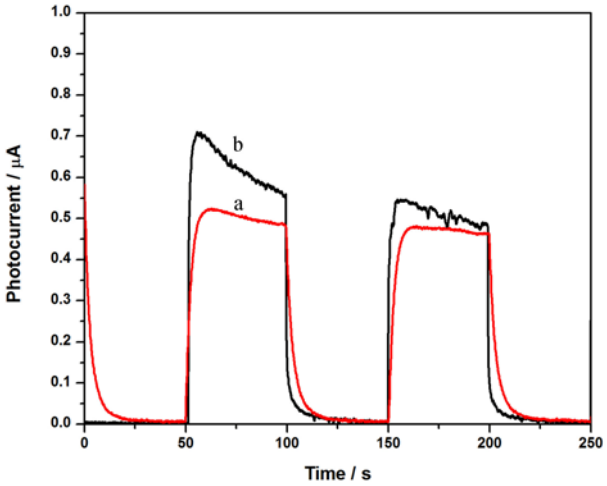

Fig. S11 Photocurrent versus time curves of the $(P_2W_{18}/TiO_2/P_2W_{18}/Au)_2$ films in different electrolyte. (a) acetonitrile, (b) 0.1M Na_2SO_4.